Title: High-throughput Automated Muropeptide Analysis (HAMA) Reveals Peptidoglycan Composition of Gut Microbial Cell Walls

Authors: Ya-Chen Hsu[1], Pin-Rui Su[1,2], Lin-Jie Huang[1], Kum-Yi Cheng[1], Chun-hsien Chen[1], Cheng-Chih Hsu[1]*

Affiliations:

[1] Department of Chemistry, National Taiwan University, Taipei 10617, Taiwan

[2] Department of Molecular Genetics, Erasmus MC, Rotterdam, Netherlands

Corresponding Author:

* Cheng-Chih Hsu

Department of Chemistry, National Taiwan University, Taipei 10617, Taiwan

+886-2-3366-3844, ccrhsu@ntu.edu.tw

ORCID: Cheng-Chih Hsu: 0000-0002-2892-5326

ABSTRACT

Peptidoglycan (PGN), a net-like polymer constituted by muropeptides, provides protection for microorganisms and has been a major target for antibiotics for decades. Researchers have explored host-microbiome interactions through PGN recognition systems and discovered key muropeptides modulating host responses. However, most common characterization techniques for muropeptides are labor-intensive and require manual analysis of mass spectra due to the complex cross-linked PGN structures. Each species has unique moiety modifications and inter-/intra-bridges, which further complicates the structural analysis of PGN. Here, we developed a high-throughput automated muropeptide analysis (HAMA) platform leveraging tandem mass spectrometry and *in silico* muropeptide MS/MS fragmentation matching to comprehensively identify muropeptide structures, quantify their abundance, and infer PGN cross-linking types. We demonstrated the effectiveness of HAMA platform using well-characterized PGNs from *E. coli* and *S. aureus* and further applied it to common gut bacteria including *Bifidobacterium, Bacteroides, Lactobacillus, Enterococcus,* and *Akkermansia muciniphila.* Specifically, we found that the stiffness and strength of the cell envelopes may correspond to the lengths and compositions of interpeptide bridges within *Bifidobacterium* species. In summary, the HAMA framework exhibits an automated, intuitive, and accurate analysis of PGN compositions, which may serve as a potential tool to investigate the post-synthetic modifications of saccharides, the variation in interpeptide bridges, and the types of cross-linking within bacterial PGNs.

33 **INTRODUCTION**

34 Peptidoglycan (PGN) is an essential and distinct component of bacterial cell walls that
35 envelop the cytoplasmic membrane.[1] It maintains a defined bacterial shape, preserves cell
36 integrity by counteracting the internal osmotic pressure, and acts as a scaffold for other cell wall-
37 anchored components such as proteins and teichoic acids.[2] Peptidoglycan provides a protective
38 barrier for microorganisms against environmental threats, contributing to its structural rigidity.
39 Generally, PGN is a net-like polymeric structure composed of liner glycan chains cross-linked by
40 short peptides. The PGN-repeat unit (so-called muropeptide) comprises *N*-acetylglucosamine
41 (GlcNAc) and *N*-acetylmuramic acid (MurNAc) linked by β1,4-glycosidic bonds and a peptide
42 stem attached to lactyl moiety of MurNAc. The stem peptide generally contains L-alanine, D-iso-
43 glutamic acid (amidated to D-iso-glutamine in most Gram-positive bacteria), *meso*-
44 diaminopimelic acid (mDAP) in Gram-negative bacteria, L-lysine in Gram-positive bacteria, D-
45 alanine, and D-alanine sequentially. In PGN architecture, portions of the stem peptide stem from
46 adjacent glycan strands are connected through transpeptidation, forming a multi-layered, three-
47 dimensional (3-D) meshwork.[3] Although this main structure is well-conserved among bacteria,
48 the mature peptidoglycan structure remains heterogeneous and species-specific. This structural
49 diversity is attributed to chemical modifications of the sugar backbone (*O*-acetylation, *N*-
50 deacetylation, and *N*-glycolylation), variations in the type of di-amino acid at position 3 of the
51 stem peptide, variations in the interpeptide bridge, and patterns of cross-linking (4-3 linkage, 3-3
52 linkage, and 2-4 linkages).[4, 5]

53 In recent years, characterizing muropeptides has become increasingly important, not only
54 because peptidoglycan is a target for antibiotic drug design, but also because of the various roles
55 muropeptides play as signaling molecules involved in microbial interaction, antimicrobial

56 release, and host innate immunity.[6-9] The gut microbiota, consisting of thousands of bacteria, is a
57 source of peptidoglycans in organisms. The signaling functions of gut microbiota-derived PGN
58 fragments in host-microbiota interactions have been extensively studied in inflammation,
59 metabolism, autoimmune diseases, and brain development.[10-13] Therefore, analyzing the PGN
60 structural composition and its chemical modifications is critical to understand the PGN
61 recognition processes and subsequent activation mechanisms in the immune system.[14]

62 Nowadays, analytical methods for peptidoglycan architecture include HPLC, LC-MS, solid-
63 state NMR, and AFM imaging, enabling a comprehensive study of PGN structure from chemical
64 composition to 3-D architecture.[5] Online ultra-performance liquid chromatography coupled with
65 electrospray ionization– tandem mass spectrometry (UPLC-ESI-MS/MS) is the primary strategy
66 for muropeptide structural identification, requiring minimal sample amounts and time.[15-17]
67 However, data processing, such as peak annotation and MS/MS spectra alignment, still relies on
68 the prior knowledge of experienced biological chemists. Previous work published by Bern et al.
69 demonstrated the analysis of muropeptides of *Clostridium difficile* with MS/MS fragmentation
70 spectra by Byonic peptide identification software.[18] Another innovative tool, PGFinder, created
71 by Patel et al., shows consistent and reproducible data analysis of Gram-negative bacterial PGN
72 with MS1 library searching.[19] Nevertheless, an automated analysis based on MS/MS
73 identification is certainly needed for a thorough PGN investigation of complex muropeptide
74 structures, particularly for gut microbial peptidoglycans.

75 Here, we developed an in-house, high-throughput automated muropeptide analysis
76 (HAMA) platform that simplifies muropeptide structures to sequence format, mimicking the
77 proteomic "bottom-up" approach. We also established a comprehensive *in silico* MS/MS
78 fragmentation database for muropeptide identification. Using this platform coupled with high-

79 resolution mass spectrometry, we revealed the peptidoglycan compositions of common gut
80 bacteria, including *Bifidobacterium, Bacteroides, Lactobacillus, Enterococcus,* and *Akkermansia*
81 *muciniphila*.

82 **MATERIAL AND METHODS**

83 **Bacterial strains and cell culture.** Bacteria and their respective media used in this work were
84 listed in Supplementary Table 1. Anaerobic bacteria such as *Bifidobacterium*, *Bacteroides,*
85 *Lactobacillus, Enterococcus,* and *Akkermansia muciniphila* were cultured anaerobically by
86 using an anaerobic workstation (Whitley DG 250, Don Whitley Scientific Limited, England).

87

88 **Peptidoglycan extraction and Mutanolysin Digestion.** The extraction of peptidoglycan was
89 performed using a previously described method, with some modifications.[9, 16] Ten milliliters of
90 overnight cultures that have reached the stationary phase were harvested and lysed by 0.5% SDS
91 solution in 0.1 M Tris/HCl (pH 7.0). After boiled for 30 min at 100 °C and thoroughly washed
92 with H_2O three times, the pellets were resuspended in 750 mL of H_2O and sonicated for 30 min.
93 The suspensions were spiked with 750 mL of 0.1 M Tris/HCl solution (pH 7.0) and treated with
94 DNase and RNase at 37 °C in a shaker for 1 hr. After the removal of residual nucleic acids, the
95 suspensions were subsequently treated with pronase to digest cell wall-bound proteins (final
96 concentration of 1 mg/mL for 16 h at the same conditions). The pronase-treated cell walls were
97 washed twice with H_2O before wall teichoic acids were released by 1 mL of 1 N HCl incubation
98 for 4 h. Insoluble peptidoglycans were washed with H_2O until pH 5-6 and resuspended in 200-
99 500 μL of 12.5 mM sodium dihydrogen-phosphate buffer (pH 5.5) to an OD_{600} of 3.0. One
100 hundred microliters of insoluble peptidoglycan suspensions were digested overnight with 1 μL of
101 mutanolysin solution (1.000 U/mL in H_2O). Following mutanolysin inactivation (100 °C boiling
102 for 3 min) and centrifugation (5 min at 10,000 rpm), the supernatants were spiked with 50 μL of
103 reduction solution (10 mg/mL sodium borohydride in 250 mM borate buffer at pH 9.0). After 20
104 min incubation at room temperature, the reduction reaction was stopped by adding 1 μL of

105 phosphoric acid (98%), resulting in pH 3-4. Reduced muropeptide samples were subsequently
106 analyzed by UPLC-MS/MS.
107
108 **UPLC-MS/MS analysis of muropeptides.** UPLC-MS/MS analysis was performed by a Dionex
109 UltiMate 3000 UHPLC system coupled to a Q-Exactive Plus hybrid quadrupole-orbitrap mass
110 spectrometer (Thermo Scientific). Soluble muropeptides were separated by an Acquity UPLC
111 CSH C18 column (130 Å, 1.7 μm, 2.1 mm × 100 mm), with a solvent A (0.1% formic acid in
112 water) and solvent B (0.1% formic acid in acetonitrile) as the mobile phase. A flow rate of 0.25
113 mL/min and 1% mobile phase B were applied in column condition. The injection volume of each
114 sample was 5 μL. An elution gradient was run for 25 min: starting with 1% solvent B for 0-2
115 min; 1-20% B (linear), 2-15 min, 20-95% B (linear), 15-17 min; 95% B, 17-19 min; 95-1% B
116 (linear), 19-21 min; 1% B, 21-25 min for re-equilibration. The column temperature was
117 controlled at 52 °C throughout the whole analysis program. A Heat electrospray ionization
118 (HESI) source was operated in positive mode, with parameters automatically optimized under a
119 flow rate of 250 μL/min (a capillary temperature of 300 °C, a probe temperature of 300 °C, and a
120 spray voltage of 3.5 kV). Data-dependent acquisition (DDA) mode was used in the instrument. A
121 mass range of MS1 acquisition was from 400 to 2,000 *m/z* at a resolution of 70,000 and the top 5
122 most abundant ions were subjected to higher-energy collision-induced dissociation (HCD)
123 fragmentation with Δ*m/z* 3 isolation window, stepped normalized collision energy (NCE) at 20,
124 25, and 35 (A.U.), and dynamic exclusion time of 4 sec.
125

126 **Data processing and data analysis.** LC-MS/MS raw data was converted to an mzXML format
127 using MSConvert (ProteoWizard) and then processed by HAMA for mass deconvolution and
128 PGN identification.
129
130 **Mutanolysin digestion assay.** Purified peptidoglycan was adjusted to OD_{600} 1.0 in sodium
131 dihydrogen-phosphate buffer and digested with 5 μL of mutanolysin (1.000 U/mL in H_2O).
132 Absorbance was measured at OD_{600} of time points at 0, 3, 6, 9, and 16 hr in a Synergy H1
133 microplate reader (BioTek) with constant orbital shaking at 37 °C.
134
135 **Immobilization of cultured bacteria for AFM imaging.** The method of bacteria
136 immobilization was performed as described previously, with some modifications.[20] Overnight
137 cultured bacteria were washed twice and diluted to OD_{600} 0.3 with 1x PBS. Freshly cleaved Si
138 wafers were coated by 500 μL of 0.1% (w/v) poly-l-lysine in H_2O and left overnight at room
139 temperature. Afterward, the substrates were rinsed five times with ultrapure H_2O and dried with a
140 nitrogen flow. One hundred microliters of the bacteria suspension were dropped on a silicon
141 substrate, left for 10-20 min, and then rinsed three times in H_2O bath. The bacteria were dried
142 onto the substrate with flowing nitrogen and rehydrated again in 1x PBS bath for liquid imaging.
143
144 **Atomic force microscopy (AFM) imaging.** Cultured bacteria images were acquired in 1x PBS
145 bath at room temperature by AFM (Dimension Icon, Bruker) with ScanAsyst™. Data were
146 collected by the PeakForce Quantitative NanoMechanics (QNM) mode with qp-CONT probes
147 (spring constant: 0.25 N/m, resonant frequency: 30 kHz, NANOSENSORS™). Images were
148 acquired at a scan rate of 25 μm/s, an applied force of 500 pN, and with a resolution of 256 × 256

149 pixels per image frame. For mechanical analysis, the approaching part of the curves were fitted
150 with the Derjaguin-Muller-Toporov (DMT) model. DMT modulus of each bacterium was
151 recorded with 16 × 16 curves on top of the bacteria with the area of 250 × 250 nm^2.

RESULTS

HAMA platform: a High-throughput Automated Muropeptide Analysis for Identification of PGN Fragments

The complex composition and structure of PGN make their structural analysis and identification a time-consuming and challenging process. To address this, we developed a high-throughput and automated platform for PGN structural analysis based on a proteomic "bottom-up" approach. Our strategy is to simplify the structure of muropeptides into sequences by which MS/MS patterns of *b*- and *y*- ions could be generated *in silico* for CID/HCD fragmentation spectra matching. The overview of peptidoglycan analysis in this work is depicted in Fig. 1a. Briefly, bacterial peptidoglycan was extracted, purified, and hydrolyzed by mutanolysin, and the muropeptide products were then analyzed by UPLC-MS/MS. The automated identification of these muropeptides was accomplished using the HAMA platform, a MATLAB-based software with a user-friendly graphic user interface (Supplementary Fig. 1) that includes three parts: *DBuilder*, *Analyzer*, and *Viewer*.

(i) ***DBuilder*** *for Species-specific muropeptide database construction.* In order to construct muropeptide databases *in silico*, inspired by the well-developed glyco-proteomics analysis, we named each residue in disaccharide peptide with a letter and simplified the muropeptide structure into a sequence format. The representation letters of monosaccharides and amino acids are listed in Supplementary Table 2. Dashes and parentheses were used to represent peptide/glycosidic bonds and discriminate certain subunits, respectively. DBuilder combined the input options of three parts (GlcNAc, MurNAc, and peptide) to generate a comprehensive database that contains monomeric, dimeric, and trimeric muropeptides, as shown in Fig. 1b. Herein, we constructed PGN multimers using two types of polymerization events: transglycosylation connected via

175 glycosidic bonds, and transpeptidation linked through peptide bonds. In DBuilder, the type of
176 peptide linkage used was the common 4-3 cross-link, which could be achieved either directly
177 through a covalent bond between the penultimate D-Ala and the third residue in the acceptor
178 peptide stem, or via an interpeptide bridge. We also considered that the terminal D-Ala (at the
179 fifth position) in the donor stem was not allowed during the transpeptidation reaction. In
180 addition, choosing more possible modifications (anhydro MurNAc residues, deacetyl GlcNAc
181 residues, acetyl MurNAc residues, and amidated iso-Glu) to construct a PGN database could lead
182 to severe mass coincidence issues for MS1 searching in the Analyzer. Hence, we set a maximum
183 modification number of six to avoid generating multi-modified muropeptide candidates. Finally,
184 the species-specific muropeptide database was outputted to a *.csv format file, including
185 muropeptide sequences and corresponding chemical formula and theoretical monoisotopic mass.

186 (ii) ***Analyzer*** *for analysis of muropeptide MS raw files.* Analyzer is an integrated tool for
187 processing MS data and identifying muropeptides. The flowchart is shown in Fig. 1c. First, the
188 species-specific database, MS raw file (mzXML format),[21] and parameters were loaded into
189 Analyzer. Parameters were originally set with MS1 range *m/z* 400-2000, retention time range 2-
190 12 min, mass tolerance of 10 ppm (orbitrap mass spectrometry data), intensity threshold of 1e5,
191 etc., which could be input by users for different experimental conditions. Then, the mzXML file
192 was processed sequentially by peak picking, deisotoping, feature selection, and deconvolution.
193 The observed masses were searched against the loaded database within 10 ppm tolerance.
194 However, in cases where the observed mass matched more than one inferred sequence in MS1
195 searching, Analyzer compared the MS/MS spectra of those MS1 matched features to *in silico*
196 MS/MS fragmentation spectra of corresponding inferred candidates through cosine similarity and
197 matched peak score (MPS= the number of the matched peaks/the number of the predicted peaks)

198 calculation. The observed mass was then identified as the sequence with the highest matching
199 score. Lastly, all identified muropeptides were merged into an Excel spreadsheet reporting
200 charge state, molecular weight, retention time, peak intensity, peak area, sequence, main scan
201 number, cosine similarity, score, etc. Analyzer also outputted a base peak chromatogram with
202 peak annotations and a result file (in Matlab data) for Viewer input. The entire analysis was
203 completed within a few minutes.

204 (iii) ***Viewer*** *for annotation and identification display.* Viewer, a visualization tool that
205 allows users to browse extracted ion chromatograms (XICs) of the identified muropeptides and
206 visualize the *in-silico* MS/MS matching spectra annotated with *b*- and *y*- ions. In the
207 muropeptide spectra match (PSM) page of each identified muropeptide, Viewer lists all inferred
208 candidates and visualizes their individual MS/MS spectral matches to clearly demonstrate the
209 process of scoring in Analyzer. Additionally, Viewer provides a data sorting function that allows
210 users to classify the identification list by molecular weight, peak area, score (in ascending or
211 descending order), and sequence (in alphabetical order).

212

213 **Demonstration of the HAMA Platform Using Well-characterized PGNs of *E. coli* and *S.***
214 ***aureus***

215 As a proof-of-concept, we demonstrated the HAMA platform using well-characterized
216 peptidoglycans from Gram-negative *Escherichia coli* DH5α and Gram-positive *Staphylococcus*
217 *aureus* SA113. The typical PGN subunit of *E. coli* is GlcNAc – MurNAc – L-Ala – D-iGlu –
218 mDAP– D-Ala – D-Ala, represented as a sequence of B-M-l(-A-E-H-A-A) in the HAMA
219 platform. For *S. aureus*, the classic PGN structure is a disaccharide-pentapeptide with the Gly_5
220 interpeptide bridge branching from the lysine, which is simplified as B-M-l(-A-Q-(G-G-G-G-G-

221)K-A-A. Based on the analyzed input dataset, approximately 70% of the peak area in the base
222 peak chromatograms was assigned to muropeptide signals, which allowed for a comprehensive
223 PGN mapping (Fig. 2a, c). The HAMA platform successfully identified *E. coli* and *S. aureus*
224 muropeptides, and their XICs and MS/MS matching spectra could be visualized in Viewer (Fig.
225 2b, d). In total, 28 and 89 unique muropeptides were identified in PGNs of *E. coli* and *S. aureus*,
226 respectively. Table 1 lists overviews of the main muropeptide peaks in the chromatograms. Upon
227 examining the entire identification results, we found that some muropeptides were eluted in
228 multiple retention times due to the existence of a few abundant stereoisomers. Additionally, a
229 few monosaccharide muropeptides identified as the loss of GlcNAc could be recognized as in-
230 source fragments by exact co-elution.

231 In the *E. coli* data, the most abundant muropeptides were disaccharide-tetrapeptide (Tetra
232 monomer) and disaccharide-tetrapeptide-disaccharide-tetrapeptide (Tetra-Tetra dimer). We also
233 identified two low-abundant muropeptides, B-M-l(-A-E-H-G) and B-M-l(-A-E-H-A-G), in
234 which the fourth and fifth Ala are individually substituted with a Gly. This unique composition
235 has been reported in strain *E. coli* Nissle 1917 from the previous analysis,[16] but not for DH5α
236 strain used in our study. In the output of *S. aureus* peptidoglycan, the elution profile was the
237 same as what has been previously known: the most abundant monomers were disaccharide-
238 pentapeptide with a $(Gly)_5$ bridge and disaccharide-pentapeptide with a Gly bridge. The most
239 abundant cross-linked dimer was disaccharide-tetrapeptide-disaccharide-pentapeptide, which
240 contains a total of ten Gly residues.[16] We also characterized the known modifications and
241 structural variations within *S. aureus* peptidoglycan, such as *O*-acetylation of MurNAc, the
242 presence of D-iGlu (non-amidated) in the stem peptides, and the length variation of the
243 interpeptide bridge. The high-throughput analysis allowed for the identification of monomeric

244 muropeptides consisting of one to nine Gly residues and dimeric muropeptides containing a total
245 of five to fourteen Gly residues in a single analysis. However, due to the insufficient structural
246 information in the peptide backbone provided by the HCD fragmentation spectra, the exact
247 number of Gly residues harbored in each PGN unit could not be determined. Hence, further
248 careful analysis and manual verification are required to confirm the identity of identified
249 muropeptides, particularly for low-score dimers and trimers. Collectively, these results provide
250 valuable insights into the PGN compositions and architectures.
251
252 **Characterizing Gut Bacterial PGN Compositions and Resolving Isomeric Muropeptides**
253 Over the past two decades, an increasing number of gut microbial species have been found
254 to be associated with human health. In addition, emerging evidence has supported the notion that
255 gut microbial muropeptides work as signaling molecules that mediate host−microbiome
256 interactions in metabolism, gut homeostasis, and immunity.[22] However, little has been discussed
257 about the structures of PGN fragments due to the diversity and complexity of gut bacterial PGNs
258 and the lack of an efficient analytical tool.[14] To date, most of the structural information on gut
259 bacterial peptidoglycan comes from reports published between 1970 to 2000,[23-25] whereas that of
260 the health-promoting gut microbes discovered in the last two decades have been rarely reported.
261 Therefore, we utilized the HAMA platform to investigate the specific PGN structures of several
262 common gut bacterial species, including *Bifidobacterium, Bacteroides, Lactobacillus,*
263 *Enterococcus,* and *Akkermansia muciiniphila*. We collected LC-MS/MS data of purified
264 peptidoglycans from ten gut bacterial species and identified those with the self-built species-
265 specific muropeptide databases. Overall, the base peak chromatograms of each species showed
266 approximately 70% of peaks were annotated as muropeptides, and these elution profiles reflected

267 the actual composition and organization within the peptidoglycan architecture. Additionally, the
268 structural compositions of these purified peptidoglycans are consistent with previous reports,
269 listed in Table 2. The muropeptide profiles of the species in this study are summarized in
270 Supplementary Table 3-12.

271 In the identification results of Gram-positive gut bacterial peptidoglycans, the main
272 muropeptide sequence is GlcNAc – MurNAc – L-Ala – D-iGln – L-Lys– D-Ala – D-Ala, in
273 which the second amino acid of the stem peptide is usually amidated to D-iGln from D-iGlu.
274 This chemical modification is done by the MurT or GatD biosynthetic enzyme and is supposed to
275 control the PGN cross-linking levels, which has recently been demonstrated using labeled PGN
276 stem mimics in certain species.[26] Another unique feature is L-ornithine (L-Orn) at the third
277 position of the stem peptide. Unlike L-lysine, which is a usual feature of Gram-positive
278 peptidoglycans, L-Orn is a non-proteinogenic amino acid and has been found in the
279 peptidoglycan of certain *Bifidobacterium* species before.[23] As anticipated, we identified the L-
280 Orn-harbored muropeptides in *B. bifidum* and *B. longum* peptidoglycans. The most species-
281 specific variation among Bifidobacterial PGN was the architecture of the interpeptide bridge,
282 such as Gly, Ser-Asp, and Ser-Ala-Thr-Ala, which corresponded to *B. breve, B. bifidum,* and *B.*
283 *longum* species. This structural diversity arouses our interest in the relationship between the
284 length of an interpeptide bridge and the physical property of the bacterial cell envelope, which
285 will be discussed in a later section.

286 In the peptidoglycans of *E. faecium* and *L. acidophilus* (Supplementary Table 4-5), we
287 observed the monomeric structure of GlcNAc – MurNAc – L-Ala – D-iGln – L-Lys– D-Ala – D-
288 Ala, which harbored an interpeptide bridge of asparagine (D-Asn) or aspartate (D-Asp),
289 shortened as B-M-l(-A-Q-(N-)K-A-A) or B-M-l(-A-Q-(D-)K-A-A). In this part, we found that

290 both B-M-l(-A-E-(N-)K) and B-M-l(-A-Q-(D-)K) had identical molecular weights since the mass
291 difference (+ 0.984 Da) between Asn (N) and Asp (D) is the same as between Gln (Q) and Glu
292 (E). This kind of isomeric muropeptides makes identification more complicated, but it can still
293 be addressed by MS/MS *in silico* fragmentation matching under an appropriate separation
294 chromatography. For example, two disaccharide-tripeptides separately eluted at 6.18 min and
295 7.02 min were found as structural isomers that existed in *E. faecium* peptidoglycan (Fig. 3 and
296 Supplementary Table 4). Through *in silico* MS/MS fragmentation matching, these two isomers
297 can be discriminated and identified as the sequences of B-M-l(-A-E-(N-)K) and B-M-l(-A-Q-(D-
298)K), respectively. To validate the correctness of the automated platform, we also extracted the
299 experimental data of those isomers and manually inspected the MS/MS spectra (Supplementary
300 Fig. 2). However, this strategy did not work for the identification of *E. faecalis* peptidoglycan
301 whose interpeptide bridge is composed of two alanine residues (Supplementary Table 3). In this
302 case, two structurally isomeric muropeptides, a disaccharide-tripeptide with a bridge (B-M-l(-A-
303 Q-(A-A-)K)) and a disaccharide-pentapeptide (B-M-l(-A-Q-K-A-A)), have similar *in silico*
304 MS/MS fragmentation patterns, which often leads to misidentification. Nevertheless, the
305 retention time still gave us information to identify them. We annotated the peak at a retention
306 time of 3.66 min as disaccharide-pentapeptide (B-M-l(-A-Q-K-A-A)) by comparing it to an
307 identical sequence that appeared in *L. acidophilus* peptidoglycan with a similar retention time
308 (3.61 min). Therefore, the other peak at a retention time of 6.39 min could be determined as
309 disaccharide-tripeptide with a bridge (B-M-l(-A-Q-(A-A-)K)), which had a longer retention time
310 than the linear structure one.

311 Apart from Gram-positive bacteria, we also analyzed the peptidoglycan of several anaerobic
312 Gram-negative bacteria, including *Bacteroides fragilis*, *Bacteroides ovatus*, *Bacteroides*

313 *thetaiotaomicron*, and *Akkermansia muciniphila* (Table 2 and Supplementary Table 9-12).
314 Structurally, the general stem peptide of Gram-negative peptidoglycan is L-Ala – D-iGlu – m-
315 DAP– D-Ala – D-Ala, with diaminopimelic acid in the third position being a representative
316 feature. The peptidoglycan structures we identified were consistent with previously published
317 ones, with *O*-acetyl-MurNAc found in *Bacteroides* species and *N*-deacetyl-GlcNAc (GlcN) in
318 *Akkermansia muciniphila*.[27, 28] The output analysis showed that around 56-66% of the total
319 muropeptides in *Bacteroides* species' peptidoglycans contained *O*-acetylated MurNAc, while
320 approximately 87% of the total muropeptides in *A. muciniphila* peptidoglycan contained de-*N*-
321 acetylated GlcNAc. The high occurrence of *N*-deacetylation in *A. muciniphila* peptidoglycan
322 suggests that *A. muciniphila* might possess a homolog of oxidative stress-induced PGN
323 deacetylase (PgdA) found in *Helicobacter pylori*.[29-31] Chemical modifications to the disaccharide
324 backbone are known to provide resistance to lysozyme and protect bacteria against enzymatic
325 attack from the host innate immune system.[32, 33]
326
327 **Inferring PGN Cross-linking Types Based on Identified PGN Fragments**
328 We not only identified peptidoglycan structures but also were dedicated to exploring the
329 type of peptide cross-linking within those gut bacterial peptidoglycan. The substrates and
330 catalyzed enzymes involved in peptide cross-linking have been targets for antibiotic development
331 and antimicrobial resistance studies.[34] In general, there are two types of PGN cross-linkage: 4-3
332 cross-links generated by D,D-transpeptidases (Ddts) and 3-3 cross-links created by L,D-
333 transpeptidases (Ldts) (see Fig. 4a). As the enzyme names imply, the substrates that Ddts and
334 Ldts bind to are terminated as D,D-stereocenters and L,D-stereocenters, which structurally
335 means pentapeptides and tetrapeptides. During D,D-transpeptidation, Ddts first remove the

336 terminal (fifth) D-Ala residue of the pentapeptide stem and form an intermediate. Then, the
337 intermediate cross-links the NH_2 group in the third position of the neighboring acceptor stem,
338 forming a 4-3 cross-link. Following this distinctive rule of PGN biosynthesis, the possible
339 combinations of 4-3 cross-linked dimers (Donor-Acceptor) are disaccharide-tetrapeptide–
340 disaccharide-pentapeptide (D45) and disaccharide-tetrapeptide–disaccharide-tetrapeptide (D44).
341 During L,D-transpeptidation, Ldts cleave the terminal (fourth) D-Ala residue of the donor
342 tetrapeptide stem and generate a peptide bond between the third residue and the NH_2 group in the
343 third position of adjacent peptide.[35] The possible structures of 3-3 cross-linked dimers are
344 disaccharide-tripeptide–disaccharide-tetrapeptide (D34) and disaccharide-tetrapeptide–
345 disaccharide-tripeptide (D33). Hence, we could infer the possible PGN cross-linkage types and
346 the involved enzymes based on the main PGN fragments.

347 Take *Bifidobacterium breve* ATCC 15700, CSCC 1900, and ATCC 15698 as examples. The
348 LC-MS profiles showed noticeable differences in muropeptide compositions among the three
349 strains (Fig. 4b). The relative muropeptide compositions of each strain are presented in a
350 heatmap (Fig. 4c). Obviously, the main muropeptides of *B. breve* ATCC 15700 are disaccharide-
351 tripeptide with an interpeptide bridge (M3b), disaccharide-tetrapeptide with an interpeptide
352 bridge (M4b), and disaccharide-tripeptide–disaccharide-tetrapeptide (D34), whereas the CSCC
353 1900 strain showed great abundances in disaccharide-tetrapeptide with an interpeptide bridge
354 (M4b), disaccharide-pentapeptide with an interpeptide bridge (M5b), and disaccharide-
355 tetrapeptide–disaccharide-tetrapeptide (D44). These results suggested that 3-3 cross-links and 4-
356 3 cross-links might be predominant in the peptidoglycans of ATCC 15700 and CSCC 1900
357 strains, respectively. In the case of ATCC 15698 strain, its peptidoglycan likely contains both

358 types of cross-links since the abundances of M3b and M4b, as well as D34 and D44, are almost
359 equivalent.

360 Broad-spectrum β-Lactams are known to inhibit D,D-transpeptidases, such as penicillin-
361 binding proteins (PBPs). However, L,D-transpeptidases are generally insensitive to β-Lactams
362 and offer alternative cross-links in the PGNs.[36] Numerous studies have investigated the role of
363 L,D-transpeptidases in the maintenance and remodeling of mature peptidoglycan in organisms
364 such as *Enterococcus faecium, Clostridium difficile, Escherichia coli,* and *Mycobacterium*
365 *tuberculosis*.[37-42] Based on the muropeptide compositional analysis mentioned above, we found
366 high abundances of M3/M3b monomer and D34 dimer in the peptidoglycans of *E. faecalis*, *E.*
367 *faecium, L. acidophilus, B. breve, B. longum,* and *A. muciniphila*, which may be the PGN
368 products catalyzed by Ldts. While the homologs of Ldts in *L. acidophilus, B. breve, B. longum,*
369 and *A. muciniphila* have been supported by genome sequence evidence,[43-46] biochemical
370 evidence is needed to confirm the existence of L,D-transpeptidases in those species.

371

372 **Proposed Bridge Length-dependent Cell Envelope Stiffness in *B. longum* and *B. breve***

373 Peptidoglycan, a protective exoskeleton around cells, provides structural integrity to the
374 cell. The porosity of the PGN scaffold, which is defined by the degree of cross-link, might affect
375 the delivery and diffusion of drugs and signaling molecules to the cell membrane. Thus,
376 modifications to PGN structure are thought to significantly influence bacterial cell mechanics.[47,
377 48] Previous evidence has indicated that a high PGN cross-linking level enhances the stiffness of
378 the cell wall material in Gram-positive bacteria.[49] The PGN-lattice architecture based on the
379 interpeptide bridge length has been investigated using solid-state NMR in *S. aureus*.[50] However,
380 the effect of the interpeptide bridge length variants on the porosity and stiffness of bacterial cell

381 envelope has little been discussed. Interestingly, the identification table presented above showed
382 that *Bifidobacterium* peptidoglycans have different architecture of the interpeptide bridges
383 among species: a tetrapeptide bridge (Ser-Ala-Thr-Ala) found in *Bifidobacterium longum* and a
384 monopeptide bridge (Gly) found in *Bifidobacterium breve* (Supplementary Fig. 3). We wondered
385 whether the length of interpeptide bridges may be related to the bacterial cell envelope's
386 mechanical properties and hypothesized that the cross-linking with shorter bridges may form a
387 tighter meshwork in peptidoglycan layers (Fig. 5a).

388 In order to explore the above relevance, we selected three *B. breve* strains and three *B.*
389 *longum* strains, whose cell morphology is similar, as research objects. The proportion of
390 muropeptide composition of these species is summarized in Fig. 5b. A slightly higher abundance
391 of peptide-linked dimers in *B. breve* than in *B. longum* implies a higher degree of PGN cross-
392 linking level in *B. breve*. Next, we directly measured the stiffness (defined by Young's modulus,
393 E) of these two species using the single-cell atomic force microscopy technique (AFM).
394 Representative data obtained on the different strains are presented in Fig. 5c. For each cell, a
395 high-resolution elasticity map was recorded on top of the cell in the central region to avoid edge
396 effects. The values of Young's modulus were extracted and subjected to statistical analysis,
397 shown in Fig. 5d. Overall for the cell envelope properties, *B. longum* displayed smaller values of
398 stiffness than *B. breve*, demonstrating softer cell envelope properties with one-fifth lower values
399 of Young's modulus. As anticipated, these data suggested the *B. breve* harboring shorter
400 interpeptide bridges corresponded to a higher cell stiffness. Furthermore, a slower hydrolysis rate
401 was observed in purified PGN of *B. breve* than in that of *B. longum*, implying that the cell wall
402 of *B. breve* is a harder exoskeleton (Supplementary Fig. 4). Interestingly, among three *B. breve*
403 strains, the average stiffness of ATCC 15700 is higher than the other strains, likely due to the

404 more abundant 3-3 cross-linkages in its peptidoglycan. Computational modeling suggested a
405 more rigid stem peptide in the conformation of L,D-cross-linking, implying the 3-3 cross-
406 linkages strengthen the PNG layer.[36, 51] These results might support our implication that a tight
407 peptidoglycan network woven with shorter peptides gives the bacterium a stiffer cell wall,
408 proposed as an idea of bridge length-dependent cell envelope.

409 **DISCUSSION**

410 The purpose of this study was to develop an automated platform for identifying and
411 analyzing the muropeptide compositions of gut bacterial PGNs. Using high-resolution MS data,
412 we characterized PGN structures of common gut microbes, investigated their PGN cross-linking
413 types, and evaluated the effect of bridge-length variants on the stiffness of bacterial cell walls.

414 In early 1970s, the amino acid compositions of PGN stem peptides were characterized in
415 many bacteria species, including certain gut microorganisms. At that time, PGNs were purified
416 and hydrolyzed under harsh acidic conditions and then separated by two-dimensional paper
417 chromatography to determine the amino acid sequence. Based on this characterization work,
418 Schleifer and Kandler proposed a bacterial PGN classification system that is still used today.[23] In
419 the *Bifidobacterium* and *Lactobacillu*s genera, only type A PGNs were identified, representing 4-
420 3 cross-linking through interpeptide bridges.[25] However, our study of *B. breve*, *B. longum*, and *L.*
421 *acidophilus* revealed a significant abundance of M3b and D34 in their muropeptide
422 compositions, implying the incorporation of 3-3 cross-linkage type within PGN network. This
423 cross-linking type is catalyzed by penicillin-insensitive L,D-transpeptidases. We speculate that
424 this finding may be due to the comprehensive mass spectrometric approaches we used.
425 Furthermore, we adopted the enzymatic method using mutanolysin to cleave the β-N-
426 acetylmuramyl-(1,4)-N-acetylglucosamine linkage, which is crucial for obtaining the complete
427 PGN subunit that preserves the original peptide linkage. Importantly, our HAMA platform
428 provides a powerful tool for mapping peptidoglycan architecture and generating structural
429 information on the PGN biosynthesis system, which is closely related to the antibiotic resistance
430 of bacteria.

431 In most Gram-positive bacteria, the interpeptide bridges vary depending on the species and
432 are likely associated with the PGN architectures. Although the chemical structure of PGN units
433 has been extensively studied, the physical structure and 3-D architecture remain open
434 questions.[52, 53] A previous review by Kim et al. suggested that the length of interpeptide bridges
435 is a key factor in determining different PGN architectures and proposed three PGN-bridge
436 length-dependent architectures based on the orientations of cross-linked peptide stems.[50] The
437 parallel-stem model, which has the smallest pore size and the highest cross-linking level, is
438 suited for bacteria with long-length bridges. The perpendicular-stem model, with intermediate
439 pore size, is proposed for bacteria with intermediate-length bridges, while the antiparallel-stem
440 model, which has the largest pore size, is for bacteria without bridges. Notably, our study
441 provides observations regarding the relationship between the bridge length and the stiffness of
442 bacterial cell walls in *Bifidobacterium* species (Fig. 5). *B. longum*, which harbors tetrapeptide
443 bridges (Ser-Ala-Thr-Ala) corresponds to lower stiffness, whereas *B. breve,* whose PGN is cross-
444 linked by monopeptide bridges (Gly), has higher stiffness. This finding implies that the PGN
445 architecture with shorter cross-linked bridges corresponds to a more rigid skeleton. This is not
446 surprising as *Bifidobacterium* species are known for their thick peptidoglycan layers, which
447 account for 30-70% of the cell wall.[35] Meanwhile, other biomolecules in the cell wall also
448 influence bacterial stiffness, such as lipoprotein, wall teichoic acids, and lipoteichoic acids.[54-57]
449 Future studies on the effect of quantitatively changing the PGN-bridge length on stiffness will
450 require intensive research, considering the cross-linking densities, glycan strand lengths, and
451 PGN architecture models. These studies may provide further insight into the physical structure
452 and architecture of PGN, which would contribute to a better understanding of the factors
453 determining bacterial cell wall properties.

454 In the HAMA platform, simplifying muropeptide structures into sequences has facilitated
455 the generation of *in silico* MS/MS fragments for spectra matching, enabling the structural
456 resolving of isomeric muropeptides. However, there are several limitations to our study design.
457 Our species-specific PGN database is built based on known structures and modifications reported
458 previously. While the identified muropeptides cover approximately 70% of peak area in the base
459 peak chromatograms, certain low-abundant muropeptides composed of uncoded amino acids or
460 saccharides required additional MS/MS identification with manual analysis. For peptide-linked
461 multimers, the current DBuilder only builds up 4-3 cross-linked sequences because including the
462 3-3 cross-link type results in severe misidentifications, as it produces similar *in silico* MS/MS
463 fragmentation patterns as the 4-3 cross-links (about 88-90% similarity). However, we can infer
464 possible PGN cross-linkages based on the type of PGN fragments obtained from hydrolysis.[58]
465 The primary limitation is that MS/MS spectra generated by HCD fragmentation carry mostly
466 structural information from disaccharide moiety (glyco-oxonium ions) without providing
467 sufficient peptide fragment ions to derive peptide sequence,[59] making it difficult to accurately
468 identify multimers and determine the position of modifications. Nevertheless, accurate
469 monoisotopic masses acquired from high-resolution mass spectrometry are still informative in
470 peptidoglycan compositional components. Alternative approaches can be considered to elucidate
471 branched structures of muropeptides, such as breaking down PGN with cell wall amidases
472 (cleaving the amide bond between MurNAc and L-Ala residue) to target stem peptide analysis,[60,
473 61] acquiring MS^3 spectra to obtain fragmentation maps, or using electron transfer dissociation
474 (ETD) fragmentation mode to leave more peptide fragments.[18] Additionally, strategies
475 commonly used in glycopeptide identification, such as multi-fragmentation modes (CID, HCD,
476 and ETD), could also be applied to PGN identification to provide more information on peptide

477 sequences and disaccharide structures.[62] To achieve a more comprehensive identification of
478 muropeptides, future maneuvers are proposed for an expanded database, innovative *in-silico*
479 fragmentation patterns, and improved MS/MS spectra acquisition.

480 HAMA is an innovative automated platform that constructs species-specific muropeptide
481 databases, validates structural identification using *in-silico* MS/MS analysis, and provides
482 visualized results for efficient and reliable identification of muropeptides, greatly reducing the
483 time-consuming task of manual interpretation of LC-MS/MS data. The HAMA platform has the
484 potential to be a valuable tool for various research fields, including microbiology, pathology,
485 molecular biology, and immunology. Its applications in identifying activation ligands for
486 antimicrobial resistance studies, characterizing key motifs recognized by pattern recognition
487 receptors for host-microbiota immuno-interaction research, and mapping peptidoglycan in cell
488 wall architecture studies. With the ease and efficiency offered by HAMA, we believe that
489 muropeptide analysis will become more accessible and contribute to a deeper understanding of
490 cell wall biology.

491 **REFERENCES**

492 1. Silhavy, T. J.; Kahne, D.; Walker, S., The bacterial cell envelope. *Cold Spring Harbor*
493 *Perspect. Biol.* **2010,** *2* (5), a000414.

494 2. Vollmer, W.; Blanot, D.; de Pedro, M. A., Peptidoglycan structure and architecture.
495 *FEMS Microbiol Rev* **2008,** *32* (2), 149–167.

496 3. Irazoki, O.; Hernandez, S. B.; Cava, F., Peptidoglycan Muropeptides: Release,
497 Perception, and Functions as Signaling Molecules. *Front Microbiol* **2019,** *10*, 500.

498 4. Schumann, P., Peptidoglycan structure. In *Methods in microbiology*, Elsevier: 2011; Vol.
499 38, pp 101-129.

500 5. Porfírio, S.; Carlson, R. W.; Azadi, P., Elucidating Peptidoglycan Structure: An
501 Analytical Toolset: (Trends in Microbiology 27, 607-622; 2019). *Trends Microbiol* **2019,**
502 *27* (7), 653-654.

503 6. Wolf, A. J.; Underhill, D. M., Peptidoglycan recognition by the innate immune system.
504 *Nat Rev Immunol* **2018,** *18* (4), 243-254.

505 7. Nikolaidis, I.; Favini-Stabile, S.; Dessen, A., Resistance to antibiotics targeted to the
506 bacterial cell wall. *Protein Sci* **2014,** *23* (3), 243-259.

507 8. Girardin, S. E.; Travassos, L. H.; Hervé, M.; Blanot, D.; Boneca, I. G.; Philpott, D. J.;
508 Sansonetti, P. J.; Mengin-Lecreulx, D., Peptidoglycan molecular requirements allowing
509 detection by Nod1 and Nod2. *J Biol Chem* **2003,** *278* (43), 41702-41708.

510 9. Huang, Y. W.; Wang, Y.; Lin, Y.; Lin, C.; Lin, Y. T.; Hsu, C. C.; Yang, T. C., Impacts of
511 Penicillin Binding Protein 2 Inactivation on β-Lactamase Expression and Muropeptide
512 Profile in Stenotrophomonas maltophilia. *mSystems* **2017,** *2* (4), e00077-00017.

513 10. Cavallari, J. F.; Fullerton, M. D.; Duggan, B. M.; Foley, K. P.; Denou, E.; Smith, B.

514 K.; Desjardins, E. M.; Henriksbo, B. D.; Kim, K. J.; Tuinema, B. R.; Stearns, J. C.;
515 Prescott, D.; Rosenstiel, P.; Coombes, B. K.; Steinberg, G. R.; Schertzer, J. D.,
516 Muramyl Dipeptide-Based Postbiotics Mitigate Obesity-Induced Insulin Resistance via
517 IRF4. *Cell Metab* **2017,** *25* (5), 1063-1074.
518 11. Inohara, N.; Ogura, Y.; Fontalba, A.; Gutierrez, O.; Pons, F.; Crespo, J.; Fukase, K.;
519 Inamura, S.; Kusumoto, S.; Hashimoto, M.; Foster, S. J.; Moran, A. P.; Fernandez-
520 Luna, J. L.; Nuñez, G., Host recognition of bacterial muramyl dipeptide mediated through
521 NOD2. Implications for Crohn's disease. *J Biol Chem* **2003,** *278* (8), 5509-5512.
522 12. Huang, Z.; Wang, J.; Xu, X.; Wang, H.; Qiao, Y.; Chu, W. C.; Xu, S.; Chai, L.;
523 Cottier, F.; Pavelka, N.; Oosting, M.; Joosten, L. A. B.; Netea, M.; Ng, C. Y. L.;
524 Leong, K. P.; Kundu, P.; Lam, K. P.; Pettersson, S.; Wang, Y., Antibody neutralization
525 of microbiota-derived circulating peptidoglycan dampens inflammation and ameliorates
526 autoimmunity. *Nat Microbiol* **2019,** *4* (5), 766-773.
527 13. Arentsen, T.; Qian, Y.; Gkotzis, S.; Femenia, T.; Wang, T.; Udekwu, K.; Forssberg,
528 H.; Diaz Heijtz, R., The bacterial peptidoglycan-sensing molecule Pglyrp2 modulates
529 brain development and behavior. *Mol Psychiatry* **2017,** *22* (2), 257-266.
530 14. Bersch, K. L.; DeMeester, K. E.; Zagani, R.; Chen, S.; Wodzanowski, K. A.; Liu, S.;
531 Mashayekh, S.; Reinecker, H. C.; Grimes, C. L., Bacterial Peptidoglycan Fragments
532 Differentially Regulate Innate Immune Signaling. *ACS Cent Sci* **2021,** *7* (4), 688-696.
533 15. Alvarez, L.; Hernandez, S. B.; de Pedro, M. A.; Cava, F., Ultra-Sensitive, High-
534 Resolution Liquid Chromatography Methods for the High-Throughput Quantitative
535 Analysis of Bacterial Cell Wall Chemistry and Structure. *Methods Mol Biol* **2016,** *1440*,
536 11-27.

537 16. Kühner, D.; Stahl, M.; Demircioglu, D. D.; Bertsche, U., From cells to muropeptide
538 structures in 24 h: peptidoglycan mapping by UPLC-MS. *Sci Rep* **2014,** *4*, 7494.
539 17. Glauner, B., Separation and quantification of muropeptides with high-performance liquid
540 chromatography. *Anal Biochem* **1988,** *172* (2), 451-464.
541 18. Bern, M.; Beniston, R.; Mesnage, S., Towards an automated analysis of bacterial
542 peptidoglycan structure. *Anal Bioanal Chem* **2017,** *409* (2), 551-560.
543 19. Patel, A. V.; Turner, R. D.; Rifflet, A.; Acosta-Martin, A. E.; Nichols, A.; Awad, M.
544 M.; Lyras, D.; Gomperts Boneca, I.; Bern, M.; Collins, M. O.; Mesnage, S., PGFinder,
545 a novel analysis pipeline for the consistent, reproducible, and high-resolution structural
546 analysis of bacterial peptidoglycans. *Elife* **2021,** *10*, e70597.
547 20. Pasquina-Lemonche, L.; Burns, J.; Turner, R. D.; Kumar, S.; Tank, R.; Mullin, N.;
548 Wilson, J. S.; Chakrabarti, B.; Bullough, P. A.; Foster, S. J.; Hobbs, J. K., The
549 architecture of the Gram-positive bacterial cell wall. *Nature* **2020,** *582* (7811), 294-297.
550 21. Chambers, M. C.; Maclean, B.; Burke, R.; Amodei, D.; Ruderman, D. L.; Neumann,
551 S.; Gatto, L.; Fischer, B.; Pratt, B.; Egertson, J.; Hoff, K.; Kessner, D.; Tasman, N.;
552 Shulman, N.; Frewen, B.; Baker, T. A.; Brusniak, M.-Y.; Paulse, C.; Creasy, D.;
553 Flashner, L.; Kani, K.; Moulding, C.; Seymour, S. L.; Nuwaysir, L. M.; Lefebvre, B.;
554 Kuhlmann, F.; Roark, J.; Rainer, P.; Detlev, S.; Hemenway, T.; Huhmer, A.;
555 Langridge, J.; Connolly, B.; Chadick, T.; Holly, K.; Eckels, J.; Deutsch, E. W.;
556 Moritz, R. L.; Katz, J. E.; Agus, D. B.; MacCoss, M.; Tabb, D. L.; Mallick, P., A cross-
557 platform toolkit for mass spectrometry and proteomics. *Nat. Biotechnol.* **2012,** *30* (10),
558 918-920.
559 22. Bastos, P. A. D.; Wheeler, R.; Boneca, I. G., Uptake, recognition and responses to

560 peptidoglycan in the mammalian host. *FEMS Microbiol. Rev.* **2020,** *45* (1), fuaa044.

561 23. Schleifer, K. H.; Kandler, O., Peptidoglycan types of bacterial cell walls and their
562 taxonomic implications. *Bacteriol Rev* **1972,** *36* (4), 407-477.

563 24. Veerkamp, J. H., The structure of the cell wall peptidoglycan of Bifidobacterium bifidum
564 var. pennsylvanicus. *Arch. Biochem. Biophys.* **1971,** *143* (1), 204-211.

565 25. Pyclik, M.; Srutkova, D.; Schwarzer, M.; Górska, S., Bifidobacteria cell wall-derived
566 exo-polysaccharides, lipoteichoic acids, peptidoglycans, polar lipids and proteins - their
567 chemical structure and biological attributes. *Int J Biol Macromol* **2020,** *147*, 333-349.

568 26. Pidgeon, S. E.; Apostolos, A. J.; Nelson, J. M.; Shaku, M.; Rimal, B.; Islam, M. N.;
569 Crick, D. C.; Kim, S. J.; Pavelka, M. S.; Kana, B. D.; Pires, M. M., L,D-Transpeptidase
570 Specific Probe Reveals Spatial Activity of Peptidoglycan Cross-Linking. *ACS Chem Biol*
571 **2019,** *14* (10), 2185-2196.

572 27. Weadge, J. T.; Clarke, A. J., Identification and characterization of O-acetylpeptidoglycan
573 esterase: a novel enzyme discovered in Neisseria gonorrhoeae. *Biochemistry* **2006,** *45* (3),
574 839-851.

575 28. Garcia-Vello, P.; Tytgat, H. L. P.; Gray, J.; Elzinga, J.; Di Lorenzo, F.; Biboy, J.;
576 Vollmer, D.; De Castro, C.; Vollmer, W.; de Vos, W. M.; Molinaro, A., Peptidoglycan
577 from Akkermansia muciniphila MucT: chemical structure and immunostimulatory
578 properties of muropeptides. *Glycobiology* **2022,** *32* (8), 712-719.

579 29. Moynihan, P. J.; Sychantha, D.; Clarke, A. J., Chemical biology of peptidoglycan
580 acetylation and deacetylation. *Bioorg Chem* **2014,** *54*, 44-50.

581 30. Wang, G.; Olczak, A.; Forsberg, L. S.; Maier, R. J., Oxidative stress-induced
582 peptidoglycan deacetylase in Helicobacter pylori. *J Biol Chem* **2009,** *284* (11), 6790-

583 6800.

584 31. Wang, G.; Maier, S. E.; Lo, L. F.; Maier, G.; Dosi, S.; Maier, R. J., Peptidoglycan
585 deacetylation in Helicobacter pylori contributes to bacterial survival by mitigating host
586 immune responses. *Infect Immun* **2010,** *78* (11), 4660-4666.

587 32. Davis, K. M.; Weiser, J. N., Modifications to the peptidoglycan backbone help bacteria to
588 establish infection. *Infect Immun* **2011,** *79* (2), 562-570.

589 33. Sychantha, D.; Brott, A. S.; Jones, C. S.; Clarke, A. J., Mechanistic Pathways for
590 Peptidoglycan O-Acetylation and De-O-Acetylation. *Front. Microbiol.* **2018,** *9*, 2332.

591 34. Srisuknimit, V.; Qiao, Y.; Schaefer, K.; Kahne, D.; Walker, S., Peptidoglycan Cross-
592 Linking Preferences of Staphylococcus aureus Penicillin-Binding Proteins Have
593 Implications for Treating MRSA Infections. *J Am Chem Soc* **2017,** *139* (29), 9791-9794.

594 35. Peltier, J.; Courtin, P.; El Meouche, I.; Lemée, L.; Chapot-Chartier, M. P.; Pons, J. L.,
595 Clostridium difficile has an original peptidoglycan structure with a high level of N-
596 acetylglucosamine deacetylation and mainly 3-3 cross-links. *J Biol Chem* **2011,** *286* (33),
597 29053-29062.

598 36. Aliashkevich, A.; Cava, F., LD-transpeptidases: the great unknown among the
599 peptidoglycan cross-linkers. *Febs j* **2022,** *289* (16), 4718-4730.

600 37. Mainardi, J. L.; Morel, V.; Fourgeaud, M.; Cremniter, J.; Blanot, D.; Legrand, R.;
601 Frehel, C.; Arthur, M.; Van Heijenoort, J.; Gutmann, L., Balance between two
602 transpeptidation mechanisms determines the expression of beta-lactam resistance in
603 Enterococcus faecium. *J Biol Chem* **2002,** *277* (39), 35801-35807.

604 38. Lecoq, L.; Dubée, V.; Triboulet, S.; Bougault, C.; Hugonnet, J. E.; Arthur, M.;
605 Simorre, J. P., Structure of Enterococcus faeciuml,d-transpeptidase acylated by ertapenem

606 provides insight into the inactivation mechanism. *ACS Chem Biol* **2013,** *8* (6), 1140-1146.
607 39. Magnet, S.; Arbeloa, A.; Mainardi, J. L.; Hugonnet, J. E.; Fourgeaud, M.; Dubost, L.;
608 Marie, A.; Delfosse, V.; Mayer, C.; Rice, L. B.; Arthur, M., Specificity of L,D-
609 transpeptidases from gram-positive bacteria producing different peptidoglycan
610 chemotypes. *J Biol Chem* **2007,** *282* (18), 13151-13159.
611 40. Sütterlin, L.; Edoo, Z.; Hugonnet, J. E.; Mainardi, J. L.; Arthur, M., Peptidoglycan
612 Cross-Linking Activity of l,d-Transpeptidases from Clostridium difficile and Inactivation
613 of These Enzymes by β-Lactams. *Antimicrob Agents Chemother* **2018,** *62* (1), e01607-
614 01617.
615 41. Magnet, S.; Dubost, L.; Marie, A.; Arthur, M.; Gutmann, L., Identification of the L,D-
616 transpeptidases for peptidoglycan cross-linking in Escherichia coli. *J Bacteriol* **2008,** *190*
617 (13), 4782-4785.
618 42. Lavollay, M.; Arthur, M.; Fourgeaud, M.; Dubost, L.; Marie, A.; Veziris, N.; Blanot,
619 D.; Gutmann, L.; Mainardi, J. L., The peptidoglycan of stationary-phase Mycobacterium
620 tuberculosis predominantly contains cross-links generated by L,D-transpeptidation. *J*
621 *Bacteriol* **2008,** *190* (12), 4360-4366.
622 43. Jeon, S.; Kim, H.; Choi, Y.; Cho, S.; Seo, M.; Kim, H., Complete Genome Sequence of
623 the Newly Developed Lactobacillus acidophilus Strain With Improved Thermal
624 Adaptability. *Front Microbiol* **2021,** *12*, 697351.
625 44. Morita, H.; Toh, H.; Oshima, K.; Nakano, A.; Omori, E.; Hattori, Y.; Arakawa, K.;
626 Suda, W.; Honda, K.; Hattori, M., Complete genome sequence of Bifidobacterium breve
627 JCM 1192(T) isolated from infant feces. *J Biotechnol* **2015,** *210*, 81-82.
628 45. Poyet, M.; Groussin, M.; Gibbons, S. M.; Avila-Pacheco, J.; Jiang, X.; Kearney, S. M.;

629 Perrotta, A. R.; Berdy, B.; Zhao, S.; Lieberman, T. D.; Swanson, P. K.; Smith, M.;
630 Roesemann, S.; Alexander, J. E.; Rich, S. A.; Livny, J.; Vlamakis, H.; Clish, C.;
631 Bullock, K.; Deik, A.; Scott, J.; Pierce, K. A.; Xavier, R. J.; Alm, E. J., A library of
632 human gut bacterial isolates paired with longitudinal multiomics data enables mechanistic
633 microbiome research. *Nat Med* **2019,** *25* (9), 1442-1452.
634 46. Ottman, N. A. Host immunostimulation and substrate utilization of the gut symbiont
635 Akkermansia muciniphila. PhD thesis, Wageningen University, Wageningen, 2015.
636 47. Auer, G. K.; Weibel, D. B., Bacterial Cell Mechanics. *Biochemistry* **2017,** *56* (29), 3710-
637 3724.
638 48. Chang, J. D.; Wallace, A. G.; Foster, E. E.; Kim, S. J., Peptidoglycan Compositional
639 Analysis of Enterococcus faecalis Biofilm by Stable Isotope Labeling by Amino Acids in
640 a Bacterial Culture. *Biochemistry* **2018,** *57* (7), 1274-1283.
641 49. Loskill, P.; Pereira, P. M.; Jung, P.; Bischoff, M.; Herrmann, M.; Pinho, M. G.; Jacobs,
642 K., Reduction of the peptidoglycan crosslinking causes a decrease in stiffness of the
643 Staphylococcus aureus cell envelope. *Biophys J* **2014,** *107* (5), 1082-1089.
644 50. Kim, S. J.; Chang, J.; Singh, M., Peptidoglycan architecture of Gram-positive bacteria by
645 solid-state NMR. *Biochim Biophys Acta* **2015,** *1848* (1 Pt B), 350-362.
646 51. de Pedro, M. A.; Cava, F., Structural constraints and dynamics of bacterial cell wall
647 architecture. *Front Microbiol* **2015,** *6*, 449.
648 52. Vollmer, W.; Seligman, S. J., Architecture of peptidoglycan: more data and more models.
649 *Trends Microbiol.* **2010,** *18* (2), 59-66.
650 53. Turner, R. D.; Vollmer, W.; Foster, S. J., Different walls for rods and balls: the diversity
651 of peptidoglycan. *Mol. Microbiol.* **2014,** *91* (5), 862-874.

652 54. Mathelié-Guinlet, M.; Asmar, A. T.; Collet, J.-F.; Dufrêne, Y. F., Lipoprotein Lpp
653 regulates the mechanical properties of the E. coli cell envelope. *Nat. Commun.* **2020,** *11*
654 (1), 1789.
655 55. Auer, G. K.; Lee, T. K.; Rajendram, M.; Cesar, S.; Miguel, A.; Huang, K. C.; Weibel,
656 D. B., Mechanical Genomics Identifies Diverse Modulators of Bacterial Cell Stiffness.
657 *Cell Syst* **2016,** *2* (6), 402-411.
658 56. Santa Maria Jr., J. P.; Sadaka, A.; Moussa, S. H.; Brown, S.; Zhang, Y. J.; Rubin, E. J.;
659 Gilmore, M. S.; Walker, S., Compound-gene interaction mapping reveals distinct roles for
660 Staphylococcus aureus teichoic acids. *Proc Natl Acad Sci U S A* **2014,** *111* (34), 12510-
661 12515.
662 57. Saar-Dover, R.; Bitler, A.; Nezer, R.; Shmuel-Galia, L.; Firon, A.; Shimoni, E.; Trieu-
663 Cuot, P.; Shai, Y., D-alanylation of lipoteichoic acids confers resistance to cationic
664 peptides in group B streptococcus by increasing the cell wall density. *PLoS Pathog* **2012,**
665 *8* (9), e1002891.
666 58. Rimal, B.; Senzani, S.; Ealand, C.; Lamichhane, G.; Kana, B.; Kim, S. J.,
667 Peptidoglycan compositional analysis of Mycobacterium smegmatis using high-
668 resolution LC-MS. *Sci Rep* **2022,** *12* (1), 11061.
669 59. Liu, G.; Cheng, K.; Lo, C. Y.; Li, J.; Qu, J.; Neelamegham, S., A Comprehensive,
670 Open-source Platform for Mass Spectrometry-based Glycoproteomics Data Analysis. *Mol*
671 *Cell Proteomics* **2017,** *16* (11), 2032-2047.
672 60. Greene, N. G.; Narciso, A. R.; Filipe, S. R.; Camilli, A., Peptidoglycan branched stem
673 peptides contribute to Streptococcus pneumoniae virulence by inhibiting pneumolysin
674 release. *PLoS Pathog.* **2015,** *11* (6), e1004996.

675 61. Biswas, R.; Voggu, L.; Simon, U. K.; Hentschel, P.; Thumm, G.; Götz, F., Activity of
676 the major staphylococcal autolysin Atl. *FEMS Microbiol. Lett.* **2006,** *259* (2), 260-268.
677 62. Reiding, K. R.; Bondt, A.; Franc, V.; Heck, A. J. R., The benefits of hybrid
678 fragmentation methods for glycoproteomics. *TrAC, Trends Anal. Chem.* **2018,** *108*, 260-
679 268.
680

681 **ACKNOWLEDGMENTS**

682 This research was supported by Ministry of Science and Technology (MOST), R.O.C.
683 (Grants MOST 108-2636-M-002-008-, 109-2636-M-002-005-, and 110-2636-M-002-014-). Y.-C.
684 H. acknowledged the financial support of "The Program of Research Performance Enhancement
685 via Students Entering Ph.D. Programs Straight from an Undergraduate/Master's Program" from
686 National Taiwan University. The instrument support from the NTU Mass Spectrometry Platform
687 was acknowledged.
688

689 **AUTHOR CONTRIBUTIONS**

690 Y.-C.H., P.-R.S., and C.-C.H. designed the experiments. P.-R.S. and Y.-C.H. built the HAMA
691 software. Y.-C.H. carried out all the MS experiments and analyzed the data. L.-J.H., K.-Y.C., and
692 C.-h.C. designed and carried out the AFM experiments. C.-C.H. supervised the study. Y.-C.H.
693 and C.-C.H. wrote the paper.
694

695 **AUTHOR INFORMATION**

696 Corresponding Author
697 * Cheng-Chih Hsu: ccrhsu@ntu.edu.tw

ORCID

Ya-Chen Hsu: 0000-0003-1202-0132

Chun-hsien Chen: 0000-0001-5507-3248

Cheng-Chih Hsu: 0000-0002-2892-5326

COMPETING INTERESTS

The authors declare no competing financial interest.

ADDITIONAL INFORMATION

Supplementary information includes supplementary figures (MS/MS spectra) and supplementary tables (lists of automated identification of gut bacterial muropeptides). The Source Data underlying Figs. 4–5 is provided as a separate Source Data file. The HAMA software package is available at: https://drive.google.com/drive/folders/17LVGOm-LEHzNmw7nPULXMEZvg_cnO3k1?usp=share_link

713 **FIGURES**

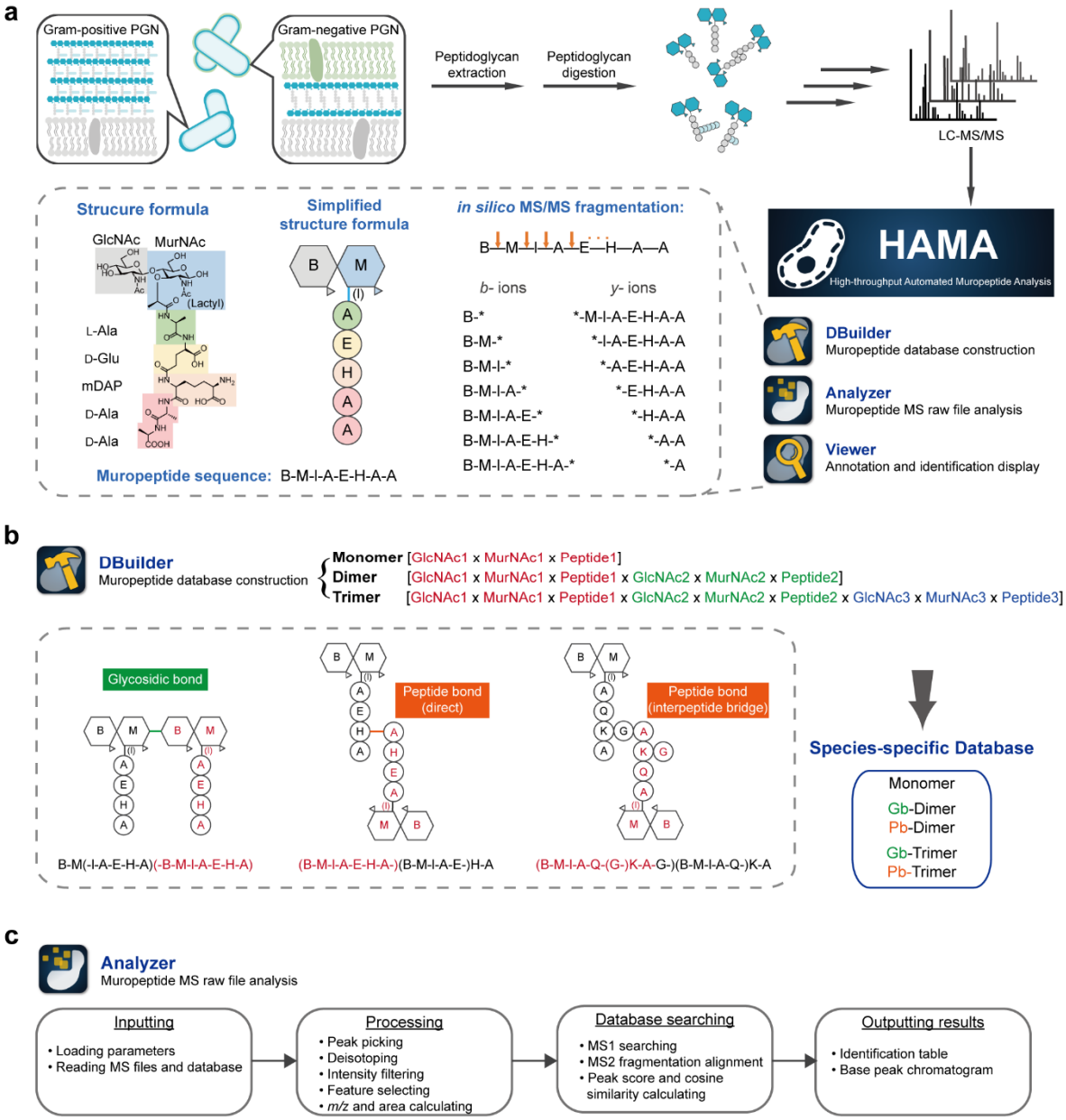

714

715 **Figure 1. Schematic representation of the high-throughput automated muropeptide**
716 **analysis (HAMA) framework.** (a) The peptidoglycans of bacteria were extracted and purified,
717 followed by mutanolysin digestion. The resulting muropeptide products are analyzed by
718 UHPLC-MS/MS and identified using the HAMA platform. The HAMA strategy involves
719 simplifying muropeptide structures to sequence format, which facilitates the database

720 construction and *in silico* generation of *b*- and *y*- ion fragmentation spectra for matching.
721 Muropeptide symbols: B, *N*-acetylglucosamine; M, *N*-acetylmuraminitol (without lactyl group);
722 l, lactic acid; A, alanine; E, glutamic acid; H, diaminopimelic acid. (b) DBuilder constructs a
723 muropeptide database containing monomers, dimers, and trimers with two types of linkage:
724 glycosidic bonds and peptide bonds. For peptide linkages, the direct way is through a direct
725 covalent bond between the penultimate D-Ala and mDAP residue in the acceptor peptide stem,
726 and the indirect way is via an interpeptide bridge branching from the lysine. Donors are labeled
727 in red, and acceptors are labeled in black. (c) The flowchart outlines the LC-MS data processing
728 in Analyzer.

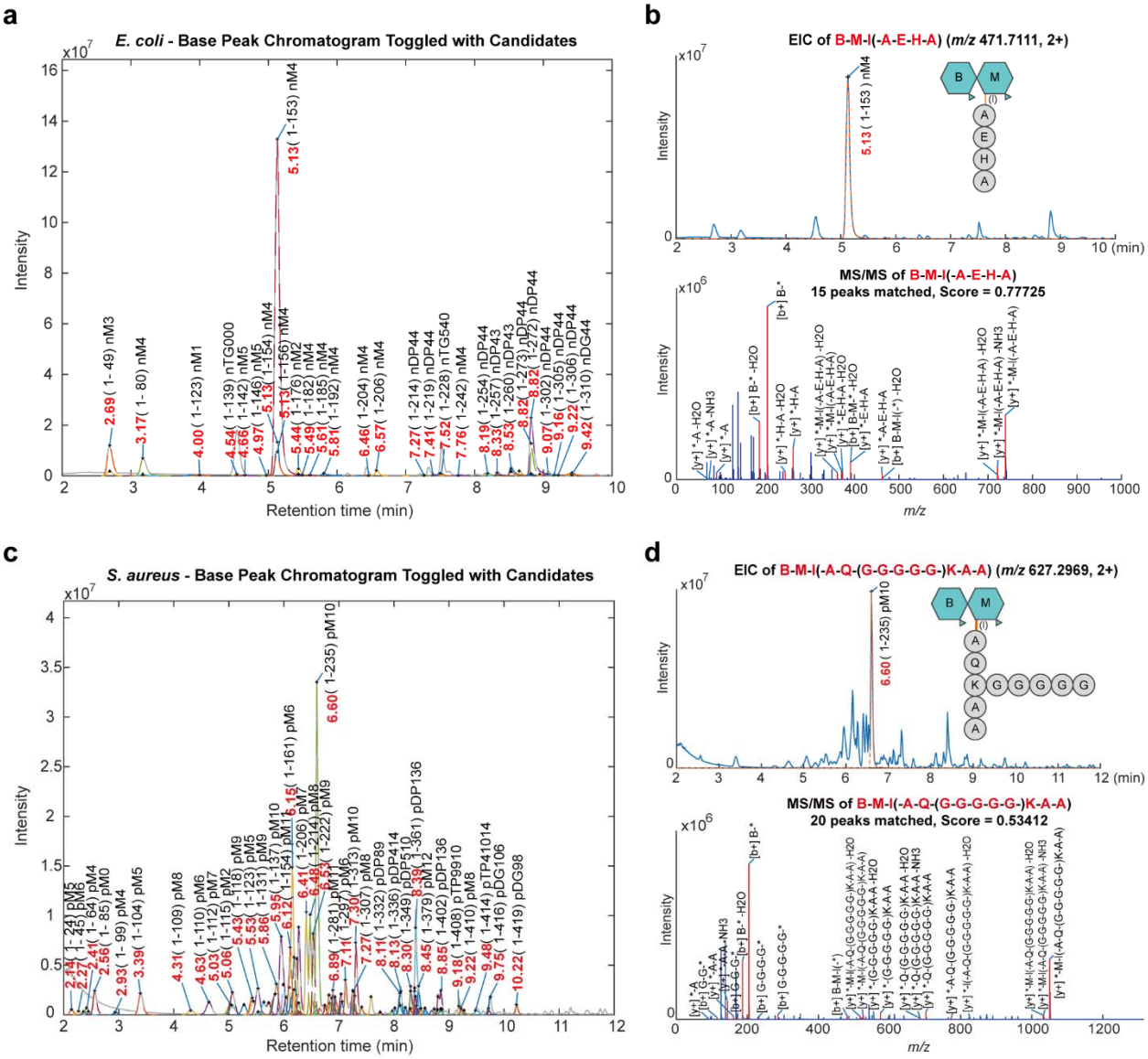

Figure 2. Automated identification of well-characterized peptidoglycans from *E. coli* and *S. aureus* using the HAMA platform. (a, c) Base peak chromatograms showing the muropeptide analysis of *E. coli* and *S. aureus*. The label content includes retention time (in red), feature index, and muropeptide class (in black). (b, d) Extracted ion chromatograms of the most abundant muropeptide and their MS/MS spectra annotated with *b*- and *y*- fragments were visualized in Viewer. Muropeptide symbols: B, N-acetylglucosamine; M, N-acetylmuraminitol (without lactyl group); l, lactic acid; A, alanine; E, glutamic acid; Q, glutamine; K, lysine; G, glycine.

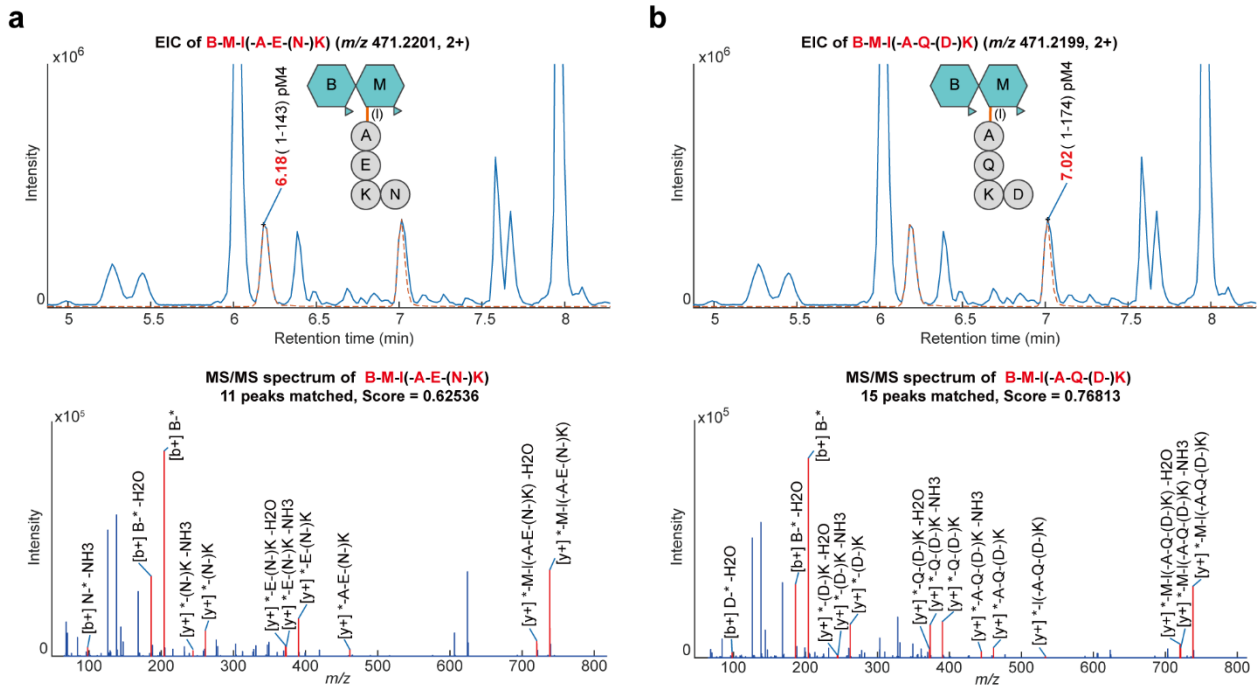

Figure 3. Resolving isomeric muropeptides by *in silico* MS/MS fragmentation matching. Two isomeric muropeptides with the same parent ion, *m/z* 471.22, were identified as two disaccharide-tripeptides: (a) B-M-l(-A-E-(N-)K eluted at 6.18 min, and (b) B-M-l(-A-Q-(D-)K eluted at 7.02 min. The sequence of each isomer was determined using *in silico* MS/MS fragmentation matching, with the identified sequence having the highest matching score. Muropeptide symbols: B, N-acetylglucosamine; M, N-acetylmuraminitol (without lactyl group); l, lactic acid; A, alanine; E, glutamic acid; Q, glutamine; K, lysine; N, Asparagine; D, Aspartic acid.

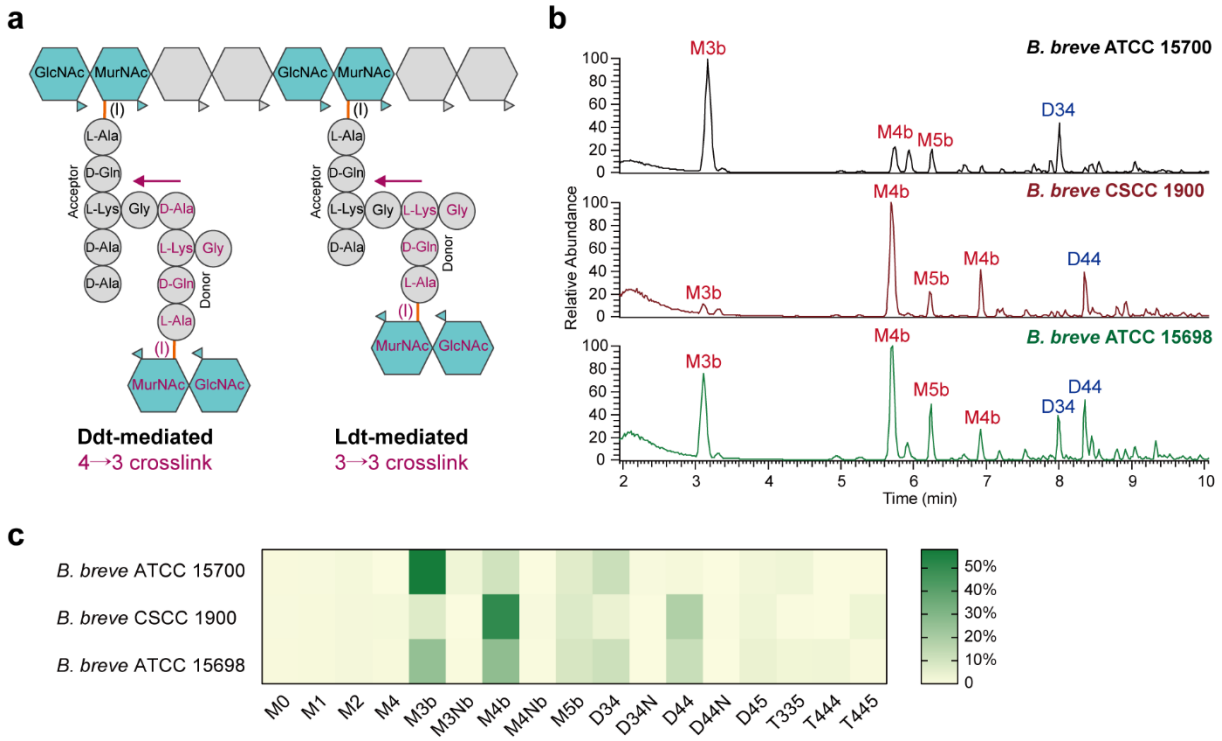

Figure 4. Muropeptide composition analysis of *Bifidobacterium breve* strains. (a) Schematic representation of the two possible cross-linking types in the PGN of *B. breve*: Ddt-mediated 4-3 cross-link and Ldt-mediated 3-3 cross-link. Donor peptide stems are labeled in red. The arrow indicates the direction of cross-links catalyzed by transpeptidases. (b) Base peak chromatograms of muropeptide analysis of *B. breve* ATCC 15700, CSCC 1900, and ATCC 15698 strains. The main peaks were annotated with muropeptide symbols. (c) Heatmap showing the muropeptide compositions (% of total) of the PGN of three *B. breve* strains. Symbols: M, monomer; D, dimer; T, trimer (numbers following the letters indicate the number of amino acids in stem peptides). M0, disaccharide; M1, disaccharide-monopeptide; M2, disaccharide-dipeptide; M4, disaccharide-tetrapeptide; M3b, disaccharide-tripeptide with an interpeptide bridge; M3Nb, disaccharide-tripeptide with an anhydro-MurNAc and an interpeptide bridge; M4b, disaccharide-tetrapeptide with an interpeptide bridge; M4Nb, disaccharide-tetrapeptide with an anhydro-MurNAc and an interpeptide bridge; M5b, disaccharide-pentapeptide with an interpeptide

760 bridge; D34, disaccharide-tripeptide–disaccharide-tetrapeptide with a peptide cross-link; D34N,
761 disaccharide-tripeptide–disaccharide-tetrapeptide with a peptide cross-link and an anhydro-
762 MurNAc; D44, disaccharide-tetrapeptide–disaccharide-tetrapeptide with a peptide cross-link;
763 D44N, disaccharide-tripeptide–disaccharide-tetrapeptide with a peptide cross-link and an
764 anhydro-MurNAc; D45, disaccharide-tetrapeptide–disaccharide-pentapeptide with a peptide
765 cross-link; T335, disaccharide-tripeptide–disaccharide-tripeptide-disaccharide-pentapeptide with
766 two peptide cross-links; T444, disaccharide-tetrapeptide–disaccharide-tetrapeptide-disaccharide-
767 tetratapeptide with two peptide cross-links; T445, disaccharide-tetrapeptide–disaccharide-
768 tetrapeptide-disaccharide-pentapeptide with two peptide cross-links.

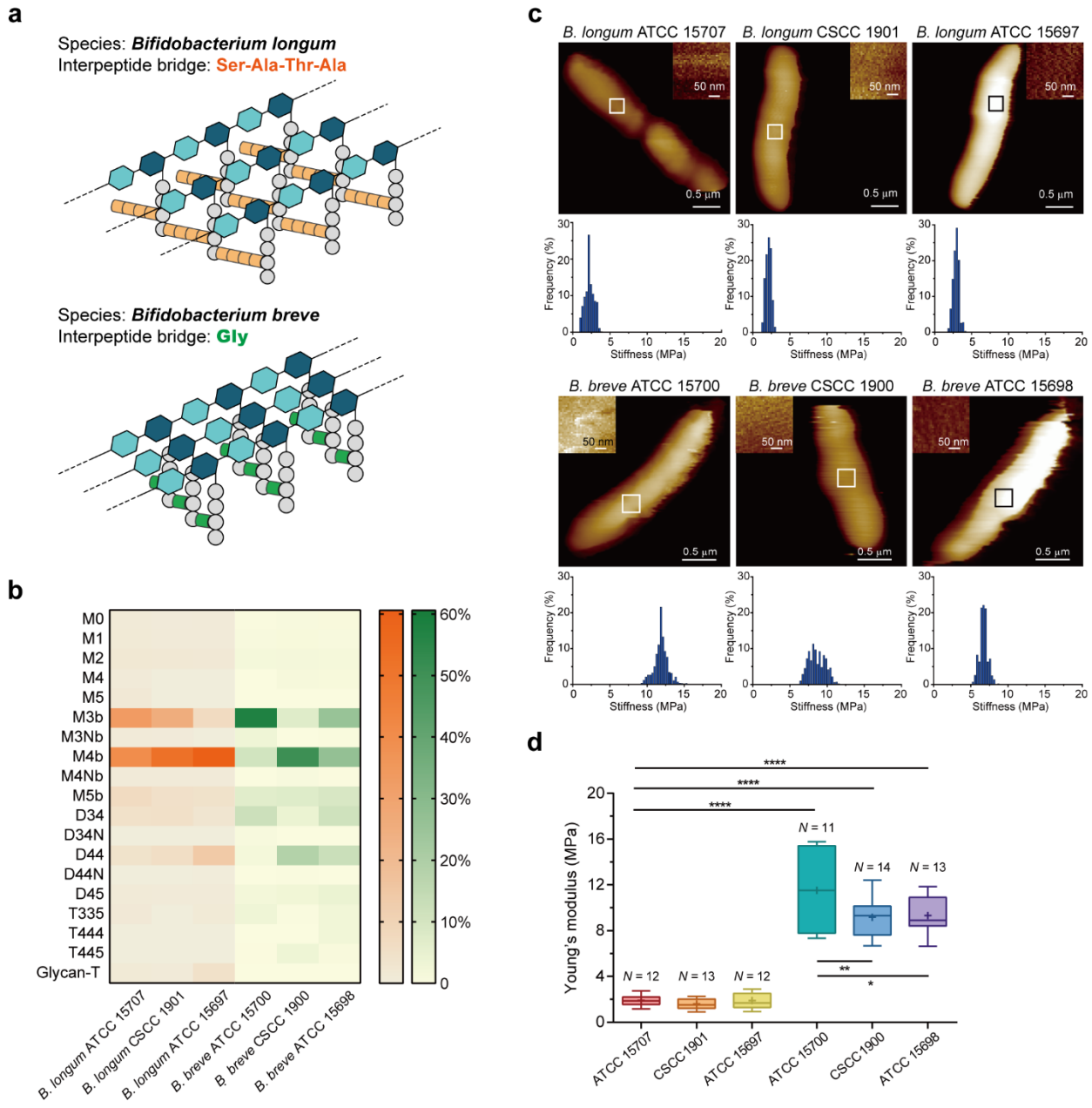

Figure 5. Bridge length-dependent cell envelope stiffness in *B. longum* and *B. breve*. (a) Schematic illustration of the Gram-positive PGN architecture of *B. longum* (orange tetrapeptide bridges) and *B. breve* (green monopeptide bridges). Glycan strands composed of repeating units of the β-1,4-linked disaccharides are cross-linked by interpeptide bridges, forming 3-D peptidoglycan layers. (b) Heatmap displaying the muropeptide compositions (% of total) of the PGNs in *B. longum* and *B. breve* (three strains each). Symbols: M, monomer; D, dimer; T, trimer

776 (numbers following the letters indicate the number of amino acids in stem peptides). M0,
777 disaccharide; M1, disaccharide-monopeptide; M2, disaccharide-dipeptide; M4, disaccharide-
778 tetrapeptide; M5, disaccharide-pentapeptide; M3b, disaccharide-tripeptide with an interpeptide
779 bridge; M3Nb, disaccharide-tripeptide with an anhydro-MurNAc and an interpeptide bridge;
780 M4b, disaccharide-tetrapeptide with an interpeptide bridge; M4Nb, disaccharide-tetrapeptide
781 with an anhydro-MurNAc and an interpeptide bridge; M5b, disaccharide-pentapeptide with an
782 interpeptide bridge; D34, disaccharide-tripeptide–disaccharide-tetrapeptide with a peptide cross-
783 link; D34N, disaccharide-tripeptide–disaccharide-tetrapeptide with a peptide cross-link and an
784 anhydro-MurNAc; D44, disaccharide-tetrapeptide–disaccharide-tetrapeptide with a peptide
785 cross-link; D44N, disaccharide-tripeptide–disaccharide-tetrapeptide with a peptide cross-link and
786 an anhydro-MurNAc; D45, disaccharide-tetrapeptide–disaccharide-pentapeptide with a peptide
787 cross-link; T335, disaccharide-tripeptide–disaccharide-tripeptide-disaccharide-pentapeptide with
788 two peptide cross-links; T444, disaccharide-tetrapeptide–disaccharide-tetrapeptide-disaccharide-
789 tetratapeptide with two peptide cross-links; T445, disaccharide-tetrapeptide–disaccharide-
790 tetrapeptide-disaccharide-pentapeptide with two peptide cross-links; Glycan-T, trimers linked by
791 glycosidic bonds. (c) AFM imaging of living *Bifidobacterium*. Topographical images in PBS
792 buffer and the inset shows elasticity images from the top of the cell. Distribution of Young's
793 modulus values corresponding to the elasticity images in the inset. (d) Statistical analysis was
794 performed for each strain, showing the distribution of two groups with the shorter interpeptide
795 bridge corresponded to higher stiffness of cell envelope. Shown here are the mean values (cross),
796 the median, and the 25 and 75% quartiles (boxes) obtained from *N* independent cells over at least
797 three independent experiments. P values were calculated using a one-way ANOVA analysis. *P ≤
798 0.05, **P ≤ 0.01, and ****P ≤ 0.0001.

799 **TABLES**

800 **Table 1. Muropeptides of *Escherichia coli DH5α* / *Staphylococcus aureus* SA113 analyzed by UPLC-MS/MS.**

	Muropeptide sequence	Retention time (min)	Class[a]	Observed MW (Da)	Theoretical MW (Da)	Δppm	Stem peptides
Escherichia coli	B-M-l(-A-E-H)	2.69	nM3	870.3711	870.3706	-0.60	Tri
	B-M-l(-A-E-H-G)	3.17	nM4	927.3918	927.3921	0.25	Tetra-Gly(4)
	B-M-l(-A-E-H-A)*	**5.13**	**nM4**	**941.4076**	**941.4077**	**0.14**	**Tetra**
	M-l(-A-E-H-A)[b]	5.13	nM4	738.3277	738.3283	0.91	Tetra
	(B-M-l-A-E-H-A-)(B-M-l-A-E-)H	8.53	nDP43	1793.7739	1793.7677	-3.43	Tri-Tetra
	(B-M-l-A-E-H-A-)(B-M-l-A-E-)H-A*	**8.82**	**nDP44**	**1864.8074**	**1864.8048**	**-1.39**	**Tetra-Tetra**
Staphylococcus aureus	B-M-l(-A-Q-K-A-A)	3.39	pM5	967.4721	967.4710	-1.20	Penta
	B-M-l(-A-Q-(G-G-G-G-G-G-)K-A)	5.95	pM10	1238.5641	1238.5626	-1.14	Tetra
	B-M-l(-A-Q-(G-)K-A-A)*	**6.15**	**pM6**	**1024.4925**	**1024.4924**	**-0.02**	**Penta**
	B-M-l(-A-Q-(G-G-G-G-G-G-G-G-)K-A)	6.18	pM12	1352.6041	1352.6056	1.12	Tetra
	B-M-l(-A-Q-(G-G-)K-A-A)	6.41	pM7	1081.5163	1081.5139	-2.26	Penta
	B-M-l(-A-Q-(G-G-G-)K-A-A)	6.48	pM8	1138.5362	1138.5354	-0.75	Penta
	B-M-l(-A-Q-(G-G-G-G-)K-A-A)	6.53	pM9	1195.5577	1195.5568	-0.71	Penta
	B-M-l(-A-Q-(G-G-G-G-G-)K-A-A)*	**6.60**	**pM10**	**1252.5806**	**1252.5783**	**-1.86**	**Penta**
	B-M-l(-A-E-(G-G-G-G-G-)K-A-A)	7.30	pM10	1253.5648	1253.5623	-2.02	Penta
	(B-M-l-A-Q-(G-G-G-G-G-)K-A-G-G-G-G-G-)(B-M-l-A-Q-)K-A-A*	**8.39**	**pDP136**	**2416.1030**	**2416.1089**	**2.44**	**Tetra-Penta**

801 a Muropeptides are cataloged by classes of Gram-negative monomer, nM, Gram-positive monomer, pM, Gram-negative dimer (peptide bond), nDP, Gram-
802 positive dimer (peptide bond), pDP, Gram-negative dimer (glycosidic bond), nDG, Gram-positive dimer (glycosidic bond), pDG, and so on. Numbers following
803 the letters are the total number of amino acids in each peptide strand.

804 [b] Monomer formed in the electrospray source by loss of monosaccharides and recognized as an in-source fragment by exact co-elution.

805 * The main products from PGN hydrolysis were labeled with bold font.

806 **Table 2. The characterized peptidoglycan types of gut bacteria used in this study.**

		Glycan backbone		Stem peptide amino acids					
Species	**Strains**	**GlcNAc**	**MurNAc**	**1**	**2**	**3**	**4**	**5**	**Interpeptide bridge** (Acceptor ← Donor)
Bifidobacterium bifidum	DSM 20082	+	+	L-Ala	D-iGln/Glu	L-Orn	D-Ala	D-Ala	D-Ser-D-Asp
Bifidobacterium breve	ATCC 15700 infant intestine	+	+	L-Ala	D-iGln/Glu	L-Lys	D-Ala	D-Ala	Gly
	CSCC 1900 nursling stools	+	+	L-Ala	D-iGln/Glu	L-Lys	D-Ala	D-Ala	Gly
	ATCC 15698 infant intestine	+	+	L-Ala	D-iGln/Glu	L-Lys	D-Ala	D-Ala	Gly
Bifidobacterium longum	ATCC 15707 adult intestine	+	+	L-Ala	D-iGln/Glu	L-Orn	D-Ala	D-Ala	L-Ser-L-Ala-L-Thr-L-Ala
	CSCC 1901 nursling stools	+	+	L-Ala	D-iGln/Glu	L-Orn/	D-Ala	D-Ala	L-Ser-L-Ala-L-Thr-L-Ala
	ATCC 15697 infant intestine	+	+	L-Ala	D-iGln/Glu	L-Orn	D-Ala	D-Ala	L-Ser-L-Ala-L-Thr-L-Ala
Lactobacillus acidophilus	ATCC 4356	+	+	L-Ala	D-iGln/Glu	L-Lys	D-Ala	D-Ala	D-iAsx (Asn+Asp)
Enterococcus faecalis	ATCC 19433	+	+	L-Ala	D-iGln/Glu	L-Lys	D-Ala	D-Ala	L-Ala-L-Ala
Enterococcus faecium	ATCC 19434	+	+	L-Ala	D-iGln/Glu	L-Lys	D-Ala	D-Ala	D-iAsx (Asn+Asp)
Bacteroides fragilis	ATCC 25285	+	*O*-acetylation	L-Ala	D-iGlu	mDAP	D-Ala	D-Ala/ Gly	-
Bacteroides ovatus	ATCC 8483	+	*O*-acetylation	L-Ala	D-iGlu	mDAP	D-Ala	D-Ala/ Gly	-
Bacteroides thetaiotaomicron	ATCC 29741	+	*O*-acetylation	L-Ala	D-iGlu	mDAP	D-Ala	D-Ala/ Gly	-
Akkermansia muciniphila	ATCC BAA-835	*N*-deacetylation	+	L-Ala	D-iGlu	mDAP	D-Ala	D-Ala/ Gly	-

807